Smart Structures and Systems, *Vol. 29, No. 5 (2022) 705-714*
https://doi.org/10.12989/sss.2022.29.5.705

Dynamic analysis of magnetorheological elastomer sandwich MEMS sensor under magnetic field

Hossein Akhavan, Javad Ehyaei* and Majid Ghadiri

Faculty of Engineering, Department of Mechanics, Imam Khomeini International University, 34148-96818, Qazvin, Iran

(*Received July 30, 2020, Revised January 13, 2022, Accepted February 23, 2022*)

Abstract. In this paper, the effect of magnetic field on the vibration behavior of a Magnetorheological elastomer (MRE) sandwich MEMS actuated by electrostatic actuation with conductive skins are examined within the multiple scales (MMS) perturbation method. Magnetorheological smart materials have been widely used in vibration control of various systems due to their mechanical properties change under the influence of different magnetic fields. To investigate the vibrational behavior of the movable electrode, the Euler-Bernoulli beam theory, as well as Hamilton's principle is used to derive the equations and the related boundary conditions governing the dynamic behavior of the system are applied. The results of this study show that by placing the Magnetorheological elastomer core in the movable electrode and applying different magnetic fields on it, its natural vibrational frequency can be affected so that by increasing the applied magnetic field, the system's natural frequency increases. Also, the effect of various factors such as the electric potential difference between two electrodes, changes in the thickness of the core and the skins, electrode length, the distance between two electrodes and also change in vibration modes of the system on natural frequencies have been investigated.

Keywords: magnetorheological elastomer; MEMS actuator; method of multiple scales; nonlinear dynamics; perturbation; sandwich beam

1. Introduction

Micro-electromechanical systems (MEMS) have a variety of applications including automotive, medical, gyroscopes and accelerometers, etc. industries. MEMS have different actuation mechanisms and it is the most important actuation is the electrostatic force because it is easy to create and consumes less energy. For this reason, in recent years, many researchers have investigated this type of micro-electromechanical actuator for use in electronic devices (Younis *et al.* 2010, Naito and Uenishi 2019, Siahpour *et al.* 2018, Pallay *et. al.* 2017, Dai *et al.* (2015). In designing movable electrodes of micro-electromechanical devices that are often modelled as beams, it is important to investigate the instability created by the application of critical voltage (Pull-in voltage). This voltage is a specific value for each micro-electromechanical system depending on various parameters such as length, width and distance of two electrodes. But in a recent study Akhavan *et al.* (2019) introduced a new model for the micro-electromechanical system and considering a sandwich electrode with a magnetorheological elastomer (MRE) core, they were able to control the pull-in voltage by applying different magnetic fields to the movable electrode. In addition to examining the pull-in voltage of MEMS systems, the study of free and forced vibration behavior and the natural frequencies of these systems are of great importance for design. Yancheng and Jianchun (2019) considered an overview of the development of smart base isolation system featuring magnetorheological elastomer. Yang *et al.* (2019) investigated the pull-in voltage and free vibration of a FGM graphene nanoplatelet (GPL) reinforced micro sandwich beams under thermo-electrical actuation. They concluded that there is an inverse relationship between the variations of the temperature with the pull-in voltage of the sandwich beam. They also concluded that the effect of temperature on natural frequencies and pull-in voltage for micro sandwich beams is greater in longer beams. Lately, researchers have been exploring various ways to control the vibrations of various structures, including beams (De Souza Eloy *et al.* 2019, Zeerouni *et al.* 2018, Priyandoko *et al.* 2018), plates (Soleymani and Arani 2019, Arumugam *et al.* 2019), and panels (Mikhasev *et al.* 2019, Asgari *et al.* 2019, Hasheminejad *et al.* 2016), and the use of the magnetorheological elastomer as the nucleus in these structures has received much attention (Hu *et al.* 2011). Nayak *et al.* (2011) investigated the vibration analysis of a sandwich beam with MRE core and two viscoelastic cores around it and then compared the experimentally and higher-order theory results. In this study, they concluded that by increasing the parameters such as the magnetic field applied to the sandwich beam, increasing the core thickness and the percentage of iron particles and carbon black used in the magnetorheological core, could reduce the instability region. In another experimental study, Guoliang *et al.* (2011) applied a non-homogeneous magnetic field to a cantilever sandwich beam with MRE core and concluded that whatever magnetic field

*Corresponding author, Ph.D.,
E-mail: jehyaei@eng.ikiu.ac.ir

ISSN: 1738-1584 (Print), 1738-1991 (Online)

was moved from the clamped end of the beam to the free end of the beam could reduce the system's natural frequencies. To improve the performance of microelectromechanical systems, it is important to investigate different structures for the movable electrode. In this context, the researchers have advanced the performance by providing a new structure with functionally graded materials for the movable electrode (Sun *et al.* 2019, Paulech *et al.* 2019, Mohammadi *et al.* 2018). However, few studies (Akhavan *et al.* 2019), have been carried out on sandwich MEMS. Gorgani *et al.* (2019) considered the instability created by the application of pull-in voltage on electrostatic NEMS/MEMS devices by considering the functionally graded materials for the movable electrode and investigated the effect of the power law index of material distribution parameter on this instability. They deduced that increasing the power law index could increase the pull-in voltage and cause the system to become unstable at higher voltages. Also, Abbasnejad *et al.* (2012) using a Galerkin based reduced- order model along with Euler-Bernoulli beam theory, studied the dynamic behavior of a FGM micro-beam made of metal and ceramic subjected to a nonlinear electrostatic force. To achieve satisfying material and economical requirements, Witvrouw *et al.* (2005) introduced a non-homogenous FGM layer to get the appropriate electrical and mechanical properties. They offered that a polycrystalline-SiGe layer was a suitable choice for MEMS. In the present study, using a new model for the movable electrode in the form of Magnetorheological elastomer (MRE) sandwich MEMS electrostatic actuator with aluminum skins under the homogeneous magnetic field, the effect of various parameters such as the electric potential difference between two electrodes, changes in the thickness of the core and the skins, electrode length, the distance between two electrodes and also change in vibration modes of the system on natural frequencies have been investigated. The authors, considering the fringing field effect, used Hamilton's principle and extracted the equations and boundary conditions governing the vibration of the movable electrode. The equations were solved using the multiple scales (MMS) perturbation method and the results were compared with the experimental and analytical results of other articles.

2. Modeling

Microelectromechanical systems are designed and manufactured in different boundary conditions that simply supported boundary condition for the design of these systems has been very important so that this boundary condition has been used in the design of MEMs microphones (Lee and Loeppert 2002), electrostatic Comb-Driven MEMS Scanning Mirror (Wang *et al*. 2021), MEMS Acoustic Emission Sensors (Ozevin 2020) and other applications. Fig. 1 shows a sandwich MEMS actuator, with two aluminum skins and an MR elastomer core of a simply supported sandwich movable electrode, with the length *L*, width *b* and thickness *h* and a fixed electrode located at a certain distance from it and a certain potential difference

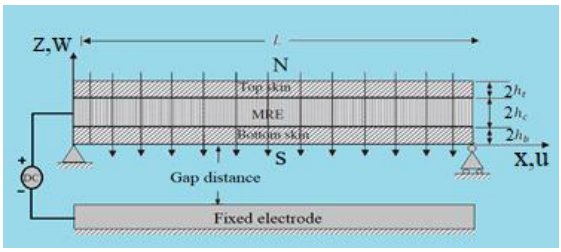

Fig. 1 MRE sandwich actuator under magnetic field, dielectric spacer, and fixed electrode

can be applied between these two electrodes. The top, bottom and core layer thickness are $2h_t$, $2h_b$ and $2h_c$ (Akhavan *et al.* (2019)), respectively. The cross-sectional areas of core, top and bottom layers are A_c, A_t and A_b, respectively. I_t and I_b denotes moment of inertia of the top and bottom skins, respectively and G_c^* denotes the complex shear modulus.

To extract the governing differential equations of vibration of the sandwich electrode, consider the following hypotheses:

1. The skins materials are homogeneous and isotropic.
2. The MRE core layer is only exposed to shear deformation.
3. At each point of the different cross-sections of the sandwich beam, the transverse displacement is considered to be the same.
4. The linkage between the layers is non-detachable and there is no possibility of slipping.
5. The transverse displacements of the upper and lower layers are equal.

Here, subscripts *t* and *b* are for top and bottom skins, respectively.

Following the results of Akhavan *et al.* (2019), and using appendix Eqs. (A1)-(A6) and applying the Hamilton's principle, the resulting non-dimensional dynamic equations of coupled transverse and axial motion and corresponding boundary conditions are

$$\left(\frac{ML^3}{D}\right)(D/E_t^*I)\frac{\partial^2\bar{w}}{\partial t^2}+(1+R)\left(\frac{D}{E_t^*I}\right)\frac{\partial^4\bar{w}}{\partial\bar{x}^4}+(R-1)D\left(\frac{B^2}{\mu_e I(E_t^*I)^2}\right)\frac{\partial^4\bar{w}}{\partial\bar{x}^4}-\left(\frac{6}{\pi}\right)D\left(\frac{B^2}{\mu_0 I(E_t^*I)^2}\right)\left(\frac{L}{h_t}\right)\ln\left(\frac{\bar{x}}{1}-\bar{x}\right)\frac{\partial^3\bar{w}}{\partial\bar{x}^3}+3D\left(\frac{B^2}{\mu_0 I(E_t^*I)^2}\right)\left(\frac{L}{h_t}\right)^2\frac{\partial^2\bar{w}}{\partial\bar{x}^2}-R\left(\frac{D}{E_t^*I}\right)\frac{\partial^3\bar{u}}{\partial\bar{x}^3}-RD\left(\frac{B^2}{\mu_e I(E_t^*)^2}\right)\frac{\partial^3\bar{u}}{\partial\bar{x}^3}=-\beta(1-\bar{w})^{-2}-\beta\gamma(1-\bar{w})^{-1} \quad (1)$$

$$\frac{\partial^3\bar{w}}{\partial\bar{x}^3}+\left(\frac{B^2}{\mu_e E_t^*}\right)\frac{\partial^3\bar{w}}{\partial\bar{x}^3}-\frac{\partial^2\bar{u}}{\partial\bar{x}^2}-\left(\frac{B^2}{\mu_e E_t^*}\right)\frac{\partial^2\bar{u}}{\partial\bar{x}^2}+G_C^*\left(\frac{1}{2E_t^*}\right)\left(\frac{L}{h_t}\right)^2\left(\frac{h_t}{h_c}\right)\bar{u}=0 \quad (2)$$

Here, B is the magnetic field applied to the sandwich beam and μ_e and μ_0 are the permeability of the skin materials and the free space, respectively. β and γ are the non-dimensional voltage and fringing field parameters, respectively and E^* is the effective Young's modulus

$$\beta=\frac{\varepsilon_0 bV^2L^4}{2IE_b^*g^3} \quad (3)$$

$$\gamma = \frac{0.65g}{b} \tag{4}$$

$$E^* = E \; for \; b \leq 5h, \tag{5}$$

$$for \; b > 5h E^* = E/(1-v^2) \tag{6}$$

and

$$D = E_t^* I_t + E_b^* I_b, \tag{7}$$

$$R = \frac{3(h_t + h_c)^2}{h_t^2} \tag{8}$$

The following non-dimensional parameters are used.

$$\bar{x} = \frac{x}{L}, \tag{9}$$

$$\bar{u} = \frac{u}{g}, \tag{10}$$

$$\bar{w} = \frac{w}{g} \tag{11}$$

Here, *w*, *u* and *x* are transverse displacement, axial displacement and independent variable of the longitudinal axis, respectively.

3. Multiple scales solution

To solve Eqs. (1) and (2), we first simplify the equations by writing the Taylor series extension of the electrostatic force around the equilibrium position, i.e., *w*=0 (Hu *et al.* 2004)

$$\begin{gathered}\left(\frac{ML^3}{D}\right)(D/E_t^* I)\frac{\partial^2 \bar{w}}{\partial t^2} + (1+R)\left(\frac{D}{E_t^* I}\right)\frac{\partial^4 \bar{w}}{\partial x^4} + (R- \\ 1)D\left(\frac{B^2}{\mu_e I(E_t^*)^2}\right)\frac{\partial^4 \bar{w}}{\partial x^4} - \left(\frac{6}{\pi}\right)D\left(\frac{B^2}{\mu_0 I(E_t^*)^2}\right)\left(\frac{L}{h_t}\right)\ln\left(\frac{\bar{x}}{1}- \right. \\ \left.\bar{x}\right)\frac{\partial^3 \bar{w}}{\partial \bar{x}^3} + 3D\left(\frac{B^2}{\mu_0 I(E_t^*)^2}\right)\left(\frac{L}{h_t}\right)^2\frac{\partial^2 \bar{w}}{\partial \bar{x}^2} - R\left(\frac{D}{E_t^* I}\right)\frac{\partial^3 \bar{u}}{\partial \bar{x}^3} - \\ RD\left(\frac{B^2}{\mu_e I(E_t^*)^2}\right)\frac{\partial^3 \bar{u}}{\partial \bar{x}^3} = -\beta(1+2w+3w^2+4w^3 333) - \\ \beta\gamma(1+w+w^2+w^3 \ldots)\end{gathered} \tag{12}$$

$$\begin{gathered}\frac{\partial^3 \bar{w}}{\partial \bar{x}^3} + \left(\frac{B^2}{\mu_e E_t^*}\right)\frac{\partial^3 \bar{w}}{\partial \bar{x}^3} - \frac{\partial^2 \bar{u}}{\partial \bar{x}^2} - \left(\frac{B^2}{\mu_e E_t^*}\right)\frac{\partial^2 \bar{u}}{\partial \bar{x}^2} + \\ G_C^*\left(\frac{1}{2E_t^*}\right)\left(\frac{L}{h_t}\right)^2(h_t/h_c)\bar{u} = 0\end{gathered} \tag{13}$$

A reduced order model achieved using the Galerkin method. Hence, the displacement functions (*w*,*u*) of the structure can be expressed as

$$w(X,t) = \sum_{i=1}^{N} \phi_i(X)\psi_i(t) \tag{14}$$

$$u(X,t) = \sum_{i=1}^{N} \phi_i'(X)\psi_i(t) \tag{15}$$

Here *N* is the number of degrees of freedom, $\phi_i(X)$ and $\phi_i'(X)$ denote the trial Eigen functions for the motion of the sandwich beam which satisfy the boundary conditions and $\Psi_i(t)$ represents the rth generalized coordinate. The mode shapes of a simply support sandwich beam can be expressed as

$$\phi_i(X) = \sin(n\pi\bar{x}) \tag{16}$$

$$\phi_i'(X) = Q\cos(n\pi\bar{x}) \tag{17}$$

Substituting Eq. (16) and Eq. (17) into Eq. (13), the coefficient Q is obtained as follows

$$Q = \frac{(n\pi)^3\left(1+(B^2/\mu_e E_t^*)\right)}{(n\pi)^2\left(1+(B^2/\mu_e E_t^*)\right) + G_c^*(1/2E_t^*)(L/h_t)^2(h_t/h_c)} \tag{18}$$

Substituting Eq. (14) and Eq. (15) into Eq. (12) and integrating with respect to x from 0 to 1 (because the longitudinal independent variable in these equations is dimensionless), we get a dif.ferential equation in terms of the coordinates $\Psi_i(t)$ as Eq. (19)

$$\begin{gathered}\left(\frac{ML^3}{D}\right)\left(\frac{D}{E_t^* I}\right)\int_0^1 \phi_i(X)\psi_i''(t)dX + (1+ \\ R)\left(\frac{D}{E_t^* I}\right)\int_0^1 \phi_i(X)^{(4)}\psi_i(t)dX + (R- \\ 1)D\left(\frac{B^2}{\mu_e I(E_t^*)^2}\right)\int_0^1 \phi_i(X)^{(4)}\psi_i(t)dX - \\ \left(\frac{6}{\pi}\right)D\left(\frac{B^2}{\mu_0 I(E_t^*)^2}\right)\left(\frac{L}{h_t}\right) \\ \int_0^1 \ln\left(\frac{\bar{x}}{1-\bar{x}}\right)\phi_i(X)^{(3)}\psi_i(t)dX + \\ 3D\left(\frac{B^2}{\mu_0 I(E_t^*)^2}\right)\left(\frac{L}{h_t}\right)^2\int_0^1 \phi_i(X)^{(2)}\psi_i(t)dX - \\ R\left(\frac{D}{E_t^* I}\right)\int_0^1 \phi_i(X)^{(3)}\psi_i(t)dX - \\ RD\left(\frac{B^2}{\mu_e I(E_t^*)^2}\right)\int_0^1 \phi_i(X)'^{(3)}\psi_i(t)dX + \\ 2\beta\int_0^1 \phi_i(X)\psi_i(t)dX + \beta\gamma\int_0^1 \phi_i(X)\psi_i(t)dX + \\ 3\beta\int_0^1 \left(\phi_i(X)\right)^2\left(\psi_i(t)\right)^2 dX + \\ 4\beta\int_0^1 \left(\phi_i(X)\right)^3\left(\psi_i(t)\right)^3 dX + \\ \beta\gamma\int_0^1 \left(\phi_i(X)\right)^3\left(\psi_i(t)\right)^3 dX + \\ \beta\gamma\int_0^1 \left(\phi_i(X)\right)^2\left(\psi_i(t)\right)^2 dX + (\beta+\beta\gamma)\int_0^1 \phi_i(X) = 0\end{gathered} \tag{19}$$

To create the orthogonality of the above integrals, multiply Eq. (19) by $\varphi_i(x)$ and we can write

Eq. (20) can be written as follows

$$\begin{gathered}(ML^3)\left(\frac{D}{E_t^* I}\right)\int_0^1 \left(\phi_t(X)\right)^2\psi_i''(t)dX + (1+ \\ R)\left(\frac{D}{E_t^* I}\right)\int_0^1 \left(\phi_t(X)\right)^{(4)}\phi_i(X)\psi_i(t)dX + (R-1)D(B^2/ \\ \mu_e I(E_t^*)^2)\int_0^1 \phi_i(X)^{(4)}\phi_i(X)\psi_i(t)dX - \\ \left(\frac{6}{\pi}\right)D\left(\frac{B^2}{\mu_0 I(E_t^*)^2}\right)\left(\frac{L}{h_t}\right) \\ \int_0^1 \ln\left(\frac{\bar{x}}{1-\bar{x}}\right)\phi_i(X)^{(3)}\phi_i(X)\psi_i(t)dX + \\ 3D\left(\frac{B^2}{\mu_0 I(E_t^*)^2}\right)\left(\frac{L}{h_t}\right)^2\int_0^1 \phi_i(X)\phi_i(X)'^{(3)}\psi_i(t)dX \\ +2\beta\int_0^1 (\phi_i(X))^2\psi_i(t)dX + \\ \beta\gamma\int_0^1 (\phi_i(X))^2\psi_i(t)dX +\end{gathered}$$

$$\begin{gathered} 3\beta \int_0^1 \left(\phi_i(X)\right)^3 (\psi_i(t))^2 dX + \\ 4\beta \int_0^1 \left(\phi_i(X)\right)^4 (\psi_i(t))^3 dX + \\ \beta\gamma \int_0^1 \left(\phi_i(X)\right)^4 (\psi_i(t))^3 dX + \\ (\beta + \beta\gamma) \int_0^1 \left(\phi_i(X)\right)^2 = 0 \end{gathered} \tag{20}$$

$$\ddot{\psi}_i + \frac{b}{a}\psi_i + \frac{e}{a}\psi_i^2 + \frac{f}{a}\psi_i^3 + d = 0 \tag{21}$$

Where the coefficient $\frac{b}{a}$ represents the vibration frequency of the system and other coefficients include nonlinear terms which can be represented by the coefficient ε as follows that ε is a small number

$$+\omega_1^2\psi_i + \mathcal{E}\alpha{\psi_i}^2 + \mathcal{E}\nabla{\psi_i}^3 + d \ = 0\ddot{\psi}_i \tag{22}$$

$$\omega_1^2 = \frac{b}{a} \tag{23}$$

$$\alpha = \frac{\mathrm{e}}{a} \tag{24}$$

$$\nabla = \frac{f}{a} \tag{25}$$

The constants a, b, d, e and f with respect to Eq (20) can be written as follows

$$a = (ML^3)(D/E_t^* I) \int_0^1 (\phi_i(X))^2 dX \tag{26}$$

$$\begin{gathered} b = (1+R)\left(\frac{D}{E_t^* I}\right) \int_0^1 \phi_i(X)^{(4)} \phi_i(X) dX - \\ \left(\frac{6}{\pi}\right) D\left(\frac{B^2}{\mu_e I (E_t^*)^2}\right)(L/h_t) \int_0^1 ln\left(\frac{\bar{x}}{1-\bar{x}}\right)\phi_i(X)^3 \phi_i(X) dX \\ +3D\left(\frac{B^2}{\mu_e I (E_t^*)^2}\right)\left(\frac{L}{h_t}\right)^2 \int_0^1 \phi_i(X)^{(2)} \phi_i(X) dX \\ +\beta\gamma \int_0^1 (\phi_i(X))^2 dX + 2\beta \int_0^1 (\phi_i(X))^2 dX \\ -R\left(\frac{D}{E_t^* I}\right) \int_0^1 \phi_i{}'(X)^{(3)} \phi_i(X) dX \end{gathered} \tag{27}$$

$$d = (\beta + \beta\gamma) \int_0^1 \phi_i(X) \tag{28}$$

$$e = (\beta\gamma + 3\beta) \int_0^1 (\phi_i(X))^3 \tag{29}$$

$$f = (\beta\gamma + 4\beta) \int_0^1 (\phi_i(X))^4 \tag{30}$$

Using the multiple scales method, the system's time response can be written as follows

$$\psi_i(T_0, T_1) = \psi_i^0(T_0, T_1) + \varepsilon\psi_i^1(T_0, T_1) \tag{31}$$

$$T_0 = t,\ T_1 = \varepsilon t \tag{32}$$

The first and second derivatives are

$$\frac{d\psi_i}{dt} = D_0\psi_i + \varepsilon D_1\psi_i = D_0\psi_i^0 + \varepsilon D_0\psi_i^1 + \varepsilon D_1\psi_i^0 \tag{33}$$

$$\frac{d^2\psi_i}{dt^2} = D_0^2\psi_i^0 + \varepsilon D_0^2\psi_i^1 + 2\varepsilon D_0 D_1\psi_i^0 \tag{34}$$

Substituting Eq. (31), Eq. (33) and Eq. (34) into Eq. (22), can be written

$$\varepsilon^0 \colon\ D_0^2\psi_i^0 + \omega_1^2\,\psi_i^0 = 0 \tag{35}$$

$$\begin{gathered} \varepsilon^1 \colon\ D_0^2\psi_i^1 + \omega_1^2\,\psi_i^1 \\ = -2D_0 D_1\psi_i^0 - \alpha{\psi_i^0}^2 - \nabla{\psi_i}^3 - d \end{gathered} \tag{36}$$

The answer to the second-order differential Eq. (35) can be written as follows

$$\psi_i^0 = A_1(T_1)e^{i\sqrt{\omega_1^2 T_0}} + A_2(T_1)e^{-i\sqrt{\omega_1^2 T_0}} \tag{37}$$

$$\begin{gathered} D_0^2\psi_i^1 + (\omega_1^2)\,\psi_i^1 = \\ (-2i\sqrt{\omega_1^2}A_1'(T_1) - 3\nabla A_1^2 A_2)e^{i\sqrt{\omega_1^2 T_0}} \\ + \left(2i\sqrt{\omega_1^2}A_2'(T_1)\right) - 3\nabla A_1 A_2^2)e^{i\sqrt{\omega_1^2 T_0}} \\ -\alpha A_1^2(T_1)e^{2i\sqrt{\omega_1^2 T_0}} - \alpha A_2^2(T_1)e^{-2i\sqrt{\omega_1^2 T_0}} \\ -2\nabla A_1(T_1)A_2(T_1) - \nabla A_1^3 e^{3i\sqrt{\omega_1^2 T_0}} \\ -\nabla A_2^2 e^{-3i\sqrt{\omega_1^2 T_0}} - d \end{gathered} \tag{38}$$

To find thez coefficients $A_1(T_1)$ and $A_2(T_1)$, Substitute Eq. (37) in Eq. (36):

Consider the secular term of Eq. (38) as zero

$$-2i\sqrt{\omega_1^2}A_1'(T_1) - 3\nabla A_1^2 A_2 = 0 \tag{39}$$

Assume $A_1(T_1)$ and $A_2(T_1)$ as follows

$$A_1 = \frac{1}{2}a(T_1)e^{i\Phi(T_1)} \tag{40}$$

$$A_2 = \frac{1}{2}a(T_1)e^{-i\Phi(T_1)} \tag{41}$$

Substituting Eq. (40) and Eq. (41) in Eq. (39) and equating zero the real and imaginary terms, $a(T_1)$ and $\Phi(T_1)$ are obtained as follows

$$\begin{gathered} a'(T_1) = 0 \\ a = a_0 \end{gathered} \tag{42}$$

$$\begin{gathered} \Phi' = \frac{3\nabla}{8\sqrt{\omega_1^2}}a^2(T_1) \\ \Phi = \frac{3\nabla}{8\sqrt{\omega_1^2}}a_0^2 T_1 + \Phi_0 \end{gathered} \tag{43}$$

Consequently, Eq. (37) can be written as follows

$$\begin{gathered} \psi_i^0 = \frac{1}{2}a_0 e^{i\left(\sqrt{\omega_1^2}T_0 + \frac{3\nabla}{8\sqrt{\omega_1^2}}a_1^2 T_1 + \Phi_0\right)} + \\ \frac{1}{2}a_0 e^{-i\left(\sqrt{\omega_1^2}T_0 + \frac{3\nabla}{8\sqrt{\omega_1^2}}a_0^2 T_1 + \Phi_0\right)} \end{gathered} \tag{44}$$

$$\psi_i^0 = a_0 \cos\left(\sqrt{\omega_1^2}T_0 + \frac{3\nabla}{8\sqrt{\omega_1^2}}a_0^2 T_1 + \Phi_0\right) \tag{45}$$

Substituting $T_0 = t$, $T_1 = \varepsilon t$ in Eq. (35), the time

Table 1 Material properties

Material	Shear modulus (MPa)	Density (gr/cm^3)	Young's modulus (GPa)
Aluminum	65.6	2.7	70
MRE	Eq. (48)	3.5	NA

Table 2 Comparison of the first natural frequency of the sandwich beam (n=1)

Magnetic field (oe)	Present study	Diff. (%)	Theoretical Sun *et al.* (2003)	Diff. (%)	Experimental Sun *et al.* (2003)
0	25.448	-18.88	22.23	-29.14	31.373
900	30	-27.14	23.24	-43.55	41.176

response and the vibration frequency of the system are obtained as follows

$$\psi_i^0 = a_0 \cos(\omega t + \Phi_0) \tag{46}$$

$$\omega = \sqrt{\omega_1^2 + \frac{3\nabla}{8\sqrt{\omega_1^2}} a_0^2 \varepsilon} \tag{47}$$

4. Results validation and discussion

To compare the results of the proposed method, we consider a sandwich beam with a smart elastomer core and Simply-support boundary conditions. The length is 400 mm, width is 25 mm, the thickness of aluminum skins are 1mm and thickness of MR core is 1 mm. Table 1 shows the required properties of the core and skins materials.

We use Eq. (48) to calculate the complex shear modulus of MR core in which the real and imaginary terms can be calculated from the following equations (Sun *et al.* 2003)

$$G_C^* = G_C' + jG_C'' \tag{48}$$

$$G_C' = (3.11 \times 10^{-7} B^2 + 3.56 \times 10^{-4} B + 5.78 \times 10^{-1}) \times 10^6 \tag{49}$$

$$G_C'' = (3.47 \times 10^{-9} B^2 + 3.85 \times 10^{-6} B + 6.31 \times 10^{-3}) \times 10^6 \tag{50}$$

Where B is the magnetic field in the Oersted unit and j=$\sqrt{-1}$. To validate the results of this study, we compare the results for the proposed sandwich beam for zero and 900 Oe magnetic field with the analytical results of the theoretical and experimental work of Sun *et al.* (2003).

We present the results and the percentage deviation between analytical and theoretical results and the experimental results in Table 2.

To increase the reliability of the results of this study, we compare the results of the natural frequencies of the system in higher mode numbers in Figs. 2-5.

As can be seen from all the results, the natural frequency increases with increasing vibration mode. As shown in Fig. 6, with increasing vibration mode, the number of vibrational

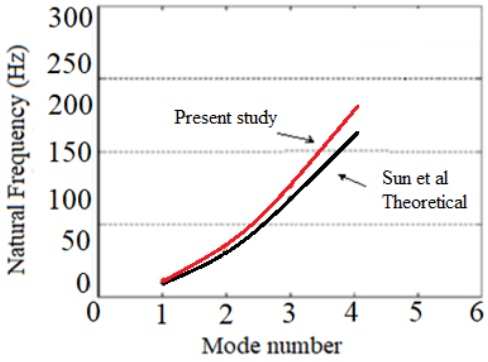

Fig. 2 Comparison between natural frequencies of present study and theoretical study of Sun *et al.* (2003) in different mode numbers in the absence of magnetic field

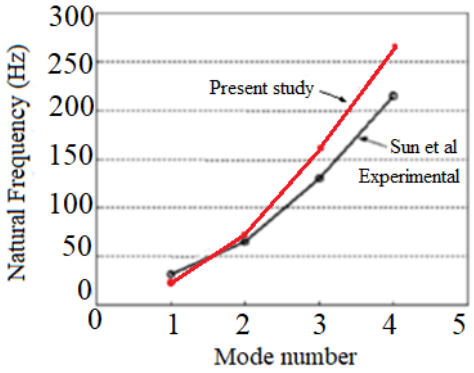

Fig. 3 Comparison between natural frequencies of present study and experimental study of Sun *et al.* (2003) in different mode numbers in the absence of magnetic field

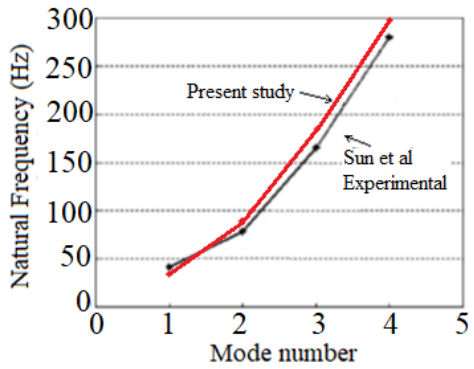

Fig. 4 Comparison between natural frequencies of present study and experimental study of Sun *et al.* (2003) in different mode numbers under magnetic field (900 Oe)

oscillations increases over a period of time, which reduces the amplitude of the oscillations and, as a result, increases the natural frequency of the system. After investigating the validity of the results of the present study, we investigate the effect of various factors such as increasing mode number, increasing applied magnetic field intensity and potential difference between two electrodes, varying the thickness of different layers of sandwich electrode, varying the length of the moving electrode and the gap distance between the two electrodes on the natural frequencies. To do this, we examine a micro sandwich beam with a smart

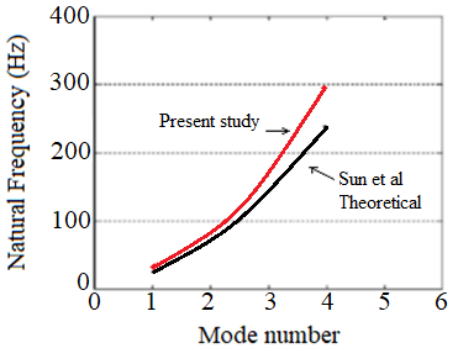

Fig. 5 Comparison between natural frequencies of present study and theoretical study of Sun *et al.* (2003) in different mode numbers under magnetic field (900 Oe)

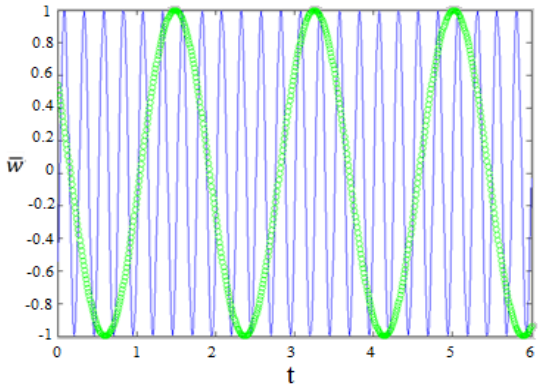

Fig. 6 Non-dimensional transverse displacement of the moving electrode in the absence of a magnetic field and potential difference for n=1 (Green circles, 25448 Hz) and n=3 (Blue lines, 180498 Hz) in x=200 μm

elastomer core and simply-support boundary conditions. The length of the micro beam is 400 μm, its width is 25 μm, the thickness of the aluminum skins is 1 μm and the thickness of the MR core is 1 μm. Also, the aluminum skins have a density of 2700 kg/m^3 and the MR core density is 3500 kg/m^3. First, we examine how the vibration mode number affects the natural frequencies of the system. Fig. 6 shows the non-dimensional transverse displacement of the moving electrode for two different modes:

In order to investigate the effect of the magnetic field on the natural frequencies of the microelectromechanical system, in two different vibrational modes, we investigate how the natural frequencies change by changing the magnetic field applied to the sandwich electrode. The shear modulus of the MRE core changes under different magnetic fields. As the magnetic field increases and the shear modulus of the core increases, the stiffness of the whole system increases and as a result the natural frequency of the system increases. Also, due to the conductivity of the skins in the proposed model, by applying a magnetic field, an magnetoelastic load is created in the skins that can increase the natural frequency of the system. Fig. 7 shows the increase of the vibration frequency of the system with the increase of the applied magnetic field in the first two-mode numbers. Microelectromechanical systems, due to their dimensions in the micron range, usually have mechanical

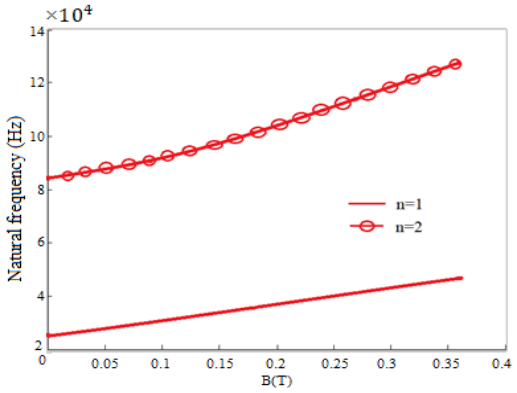

Fig. 7 The first two natural frequencies versus magnetic field in two different mode numbers

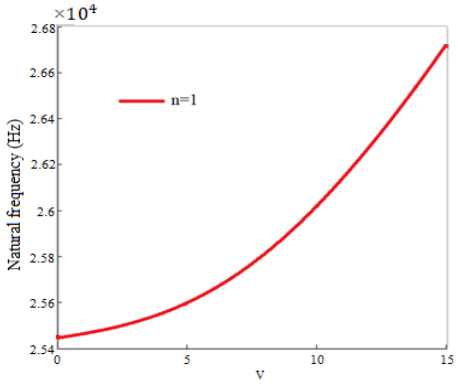

Fig. 8 The first natural frequency versus voltage (n=1)

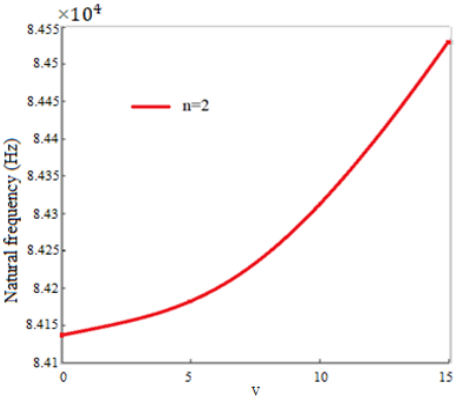

Fig. 9 The second natural frequency versus voltage (n=2)

Table 3 The natural frequency versus voltage in the first two-mode numbers

Mode number	Voltage (v)			
	0	5	10	15
1	25448.2(Hz)	25592.08(Hz)	26018.96(Hz)	26715.34(Hz)
2	84136.94(Hz)	84180.57(Hz)	84311.33(Hz)	84528.80(Hz)

resonant frequencies in the range from kHz to MHz, and even GHz (Lin and Wang 2006), which can be used in different applications such as high-frequency MEMs accelerometers.

Figs. 8-9 indicate an increase in the first two natural

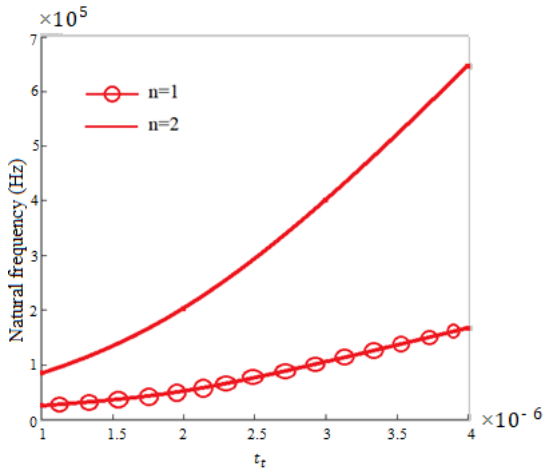

Fig. 10 The first two natural frequencies versus top layer thickness

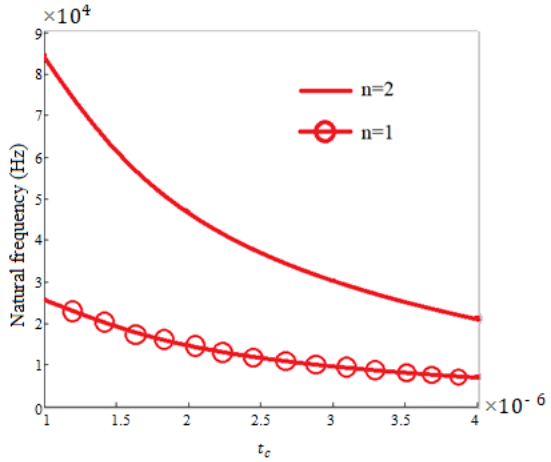

Fig. 11 The first two natural frequencies versus MR core thickness

Table 4 The first two natural frequencies versus MR core thickness

	MR core thickness			
Mode number	t_c =1 μm	t_c =2 μm	t_c =3 μm	t_c =4 μm
1	25448.20 (Hz)	14480.69 (Hz)	9563.80 (Hz)	6880.39 (Hz)
2	84136.94 (Hz)	46808.09 (Hz)	30083.77 (Hz)	21093.01 (Hz)

Table 5 The first two natural frequencies versus top layer thickness

	Top layer thickness			
Mode number	t_t =1 μm	t_t =2 μm	t_t =3 μm	t_t =4 μm
1	25448.20 (Hz)	54323.54 (Hz)	104251.25 (Hz)	165858.17 (Hz)
2	84136.94 (Hz)	202280.68 (Hz)	400464.07 (Hz)	645445.34 (Hz)

frequencies due to the increase in the applied potential difference between two electrodes. The results are also presented in Table 3.

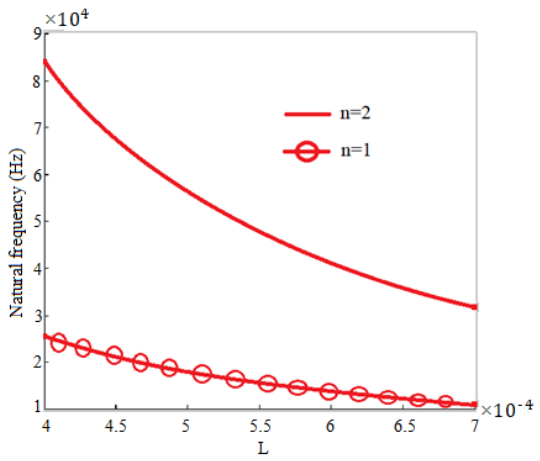

Fig. 12 The first two natural frequencies versus the length

Table 6 The first two natural frequencies versus movable electrode length

	Movable electrode length			
Mode number	L =400 μm	L =500 μm	L =600 μm	L =700 μm
1	25448.20 (Hz)	17979.94 (Hz)	13697.15 (Hz)	10945.83 (Hz)
2	84136.94 (Hz)	56229.01 (Hz)	40940.61 (Hz)	31607.06 (Hz)

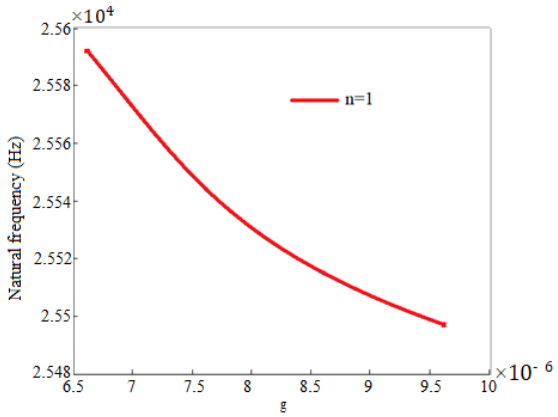

Fig. 13 The first natural frequency versus gap distance (n=1)

In order to investigate the effect of thickness variation of the aluminum top and bottom skins and MR core on the first two natural frequencies of the system, we study how the thicknesses changes affect the natural frequencies. Figs. 10-11 and Tables 4-5 show the natural frequencies increase with increasing skins thickness and the system natural frequencies decrease with increasing MR core thickness in the first two vibrational modes.

To investigate the effect of changing the length of the moving electrode on the natural frequencies of the microelectromechanical system, we study how the natural frequencies change with an increase in the length of the electrode. Fig. 12 shows the natural frequency decrease of the system by increasing the length in the first two modes because the stiffness of the system decreases, Also the results are reported in Table 6.

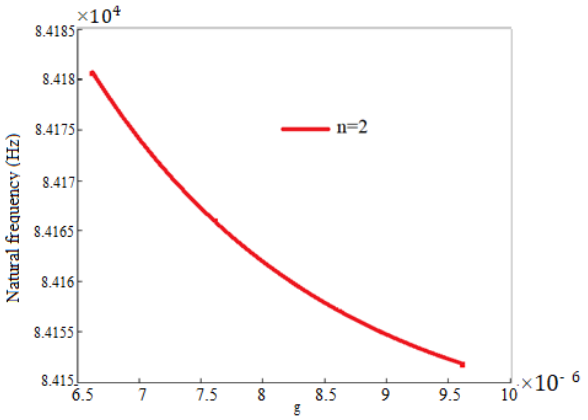

Fig. 14 The second natural frequency versus gap distance (n=2)

Figs. 13-14 indicate a decrease in the natural frequencies due to the increase in the gap distance between two electrodes because increasing the distance between two electrodes can reduce the electrostatic force created between these two electrodes.

The results are also presented in Table7.

5. Conclusions

In this work, the first two natural frequencies of a sandwich simply-support MEMS actuator under the influence of different magnetic fields and the effect of the applied potential difference have been considered using classical sandwich beam theory. The results of this study show the influence of various factors on the natural frequencies of the system as follows:

- By increasing the magnetic field applied to the sandwich electrode at all vibrational modes, the natural frequencies of the system increases.
- By increasing the applied potential difference between two electrodes at all vibrational modes, the natural frequencies of the system increase.
- It can be seen that the change in the MRE core thickness has a reverse effect than the change in the skin's thickness on natural frequency.
- The results show that increasing the length of the electrode as well as increasing the gap distance between the two electrodes decreases the natural frequencies of the system.

Table 7 The first two natural frequencies versus gap distance

Mode number	Gap distance			
	g =6.62 μm	g =7.62 μm	g =8.62 μm	g =9.62 μm
1	25592.08 (Hz)	25543.73 (Hz)	25514.99 (Hz)	25496.81 (Hz)
2	84180.57 (Hz)	84165.89 (Hz)	84157.17 (Hz)	84151.66 (Hz)

References

Abbasnejad, B. and Rezazadeh, G. (2012), "Mechanical behavior of a FGM micro-beam subjected to a nonlinear electrostatic pressure", *Int. J. Mech. Mater. Des.*, **8**(4), 381-392. https://doi.org/10.1007/s10999-012-9202-x.

Arumugam, A.B., Ramamoorthy, M. and Rajamohan, V. (2019), "Dynamic characterization and parametric instability analysis of rotating magnetorheological fluid composite sandwich plate subjected to periodic in-plane loading", *J. Sandw. Struct. Mater.*, **21**(6), 2099-2126. https://doi.org/10.1177/1099636218762690.

Akhavan, H., Ghadiri, M. and Zajkani, A. (2019), "A new model for the cantilever MEMS actuator in magnetorheological elastomer cored sandwich form considering the fringing field and Casimir effects", *Mech. Syst. Signal Pr.*, **121**, 551-561. https://doi.org/10.1016/j.ymssp.2018.11.046.

Asgari, M., Rayyat Rokn-Abadi, M., Yousefi, M. and Haddadpour, H. (2019), "Aeroelastic analysis of a sandwich panel with partially treated magneto-rheological fluid core", *J. Intel. Mater. Syst. Struct.*, **30**(1), 140-154. https://doi.org/10.1177/1045389X18803462.

Dai, H.L., Wang, L. and Ni, Q. (2015), "Dynamics and pull-in instability of electrostatically actuated microbeams conveying fluid", *Microfluid. Nanofluid.*, **18**(1), 49-55. https://doi.org/10.1007/s10404-014-1407-x.

De Souza Eloy, F., Gomes, G.F., Ancelotti Jr. A.C., Da Cunha Jr. S.S., Bombard, A.J.F. and Junqueira, D.M. (2019), "A numerical-experimental dynamic analysis of composite sandwich beam with magnetorheological elastomer honeycomb core", *Compos. Struct.*, **209**, 242-257. https://doi.org/10.1016/j.compstruct.2018.10.041.

Farrokhabadi, A., Mohebshahedin, A., Rach, R. and Duan, J.S. (2016), "An improved model for the cantilever NEMS actuator including the surface energy, fringing field and Casimir effectstrs", *Phys. E Low Dimen. Syst. Nanouct.*, **75**, 202-209. https://doi.org/10.1016/j.physe.2015.09.033.

Gorgani, H.H., Adeli, M.M. and Hosseini, M. (2019), "Pull-in behavior of functionally graded micro/nano-beams for MEMS and NEMS switches", *Microsyst. Technol.*, **25**(8), 3165-3173. https://doi.org/10.1007/s00542-018-4216-4.

Guoliang, H., Miao, G. and Weihua, L. (2011), "Analysis of vibration characteristics of magnetorheological elastomer sandwich beam under non-homogeneous magnetic field", *Appl. Mech. Mater.*, **101-102**, 202-206. https://doi.org/10.4028/www.scientific.net/AMM.101-102.202.

Hasheminejad, S.M., Parvasi, S.M. and Fadavi-Ardakani, A. (2016), "Vibroacoustic analysis and response suppression of a rectangular sandwich electrorheological panel", *Int. J. Acoust. Vib.*, **21**(1), 81-92. https://doi.org/10.20855/ijav.2016.21.1398.

Hu, G., Guo, M., Li, W., Du, H. and Alici, G. (2011), "Experimental investigation of the vibration characteristics of a magnetorheological elastomer sandwich beam under non-homogeneous small magnetic fields", *Smart Mater. Struct.*, **20**(12), 127001. https://doi.org/10.1088/0964-1726/20/12/127001.

Huang, J.M., Liew, K.M., Wong, C.H., Rajendran, S., Tan, M.J. and Liu, A.Q. (2001), "Mechanical design and optimization of capacitive micromachined switch", *Sensor. Actuat. A Phys.*, **93**(3), 273-285. https://doi.org/10.1016/S0924-4247(01)00662-8.

Hu, Y.C., Chang, C.M. and Huang, S.C. (2004), "Some design considerations on the electrostatically actuated microstructures", *Sensor. Actuat. A Phys.*, **112**(1), 155-161. https://doi.org/10.1016/j.sna.2003.12.012.

Lee, S.B. and Loeppert, P.V. (2002), "An impedance spectroscopic study of MEMS microphones", *SENSORS*, **2**, 1250-1255. https://doi.org/10.1109/ICSENS.2002.1037295.

Lin, R.M. and Wang, W.J. (2006), "Structural dynamics of

microsystems-Current state of research and future directions", *Mech. Syst. Signal Pr.*, **20**(5), 1015-1043. https://doi.org/10.1016/j.ymssp.2005.08.013.

Mikhasev, G.I., Eremeyev, V.A., Wilde, K. and Maevskaya, S.S. (2019), "Assessment of dynamic characteristics of thin cylindrical sandwich panels with magnetorheological core", *J. Intel. Mater. Syst. Struct.*, **30**(18-19), 2748-2769. https://doi.org/10.1177/1045389X19873423.

Mohammadi, M., Eghtesad, M. and Mohammadi, H. (2018), "Stochastic analysis of pull-in instability of geometrically nonlinear size-dependent FGM micro beams with random material properties", *Compos. Struct.*, **200**, 466-479. https://doi.org/10.1016/j.compstruct.2018.05.089.

Nayak, B., Dwivedy, S.K. and Murthy, K.S.R.K. (2011), "Dynamic analysis of magnetorheological elastomer-based sandwich beam with conductive skins under various boundary conditions", *J. Sound Vib.*, **330**(9), 1837-1859. https://doi.org/10.1016/j.jsv.2010.10.041.

Naito, Y. and Uenishi, K. (2019), "Electrostatic MEMS Vibration Energy Harvesters inside of Tire Treads", *Sensor.*, **19**(4), 890. https://doi.org/10.3390/s19040890.

Ozevin, D. (2020), "MEMS acoustic emission sensors", *Appl. Sci.*, **10**(24), 8966. https://doi.org/10.3390/app10248966.

Pallay, M., Daeichin, M. and Towfighian, S. (2017), "Dynamic behavior of an electrostatic MEMS resonator with repulsive actuation", *Nonlin. Dyn.*, **89**(2), 1525-1538. https://doi.org/10.1007/s11071-017-3532-z.

Paulech, J., Murín, J., Kutiš, V. and Gálik, G. (2019), "Analysis of FGM actuator structure using new multiphysical finite elements", *AIP Conf. Proc.*, **2131**(1), 020034. https://doi.org/10.1063/1.5119487.

Priyandoko, G., Kurniawan, T. and Soffie, S.M. (2018), "Vibration control of magnetorheological elastomer beam sandwich", *Proc. Electr. Eng. Comput. Sci. Inform.*, **5**(5), 341-344. https://doi.org/10.11591/eecsi.v5.1629.

Siahpour, S., Zand, M.M. and Mousavi, M. (2018), "Dynamics and vibrations of particle-sensing MEMS considering thermal and electrostatic actuation", *Microsyst. Technol.*, **24**(3), 1545-1552. https://doi.org/10.1007/s00542-017-3554-y.

Soleymani, T. and Arani, A.G. (2019), "On aeroelastic stability of a piezo-MRE sandwich plate in supersonic airflow", *Compos. Struct.*, **230**, 111532. https://doi.org/10.1016/j.compstruct.2019.111532.

Sun, Y., Cheng, J., Wang, Z., Yu, Y., Tian, L. and Lu, J. (2019), "Analytical approximate solution for nonlinear behavior of cantilever FGM MEMS beam with thermal and size dependency", *Math. Prob. Eng.*, **2019**(4), 1-10. https://doi.org/10.1155/2019/9637048.

Sun, Q., Zhou, J. and Zhang, L. (2003), "An adaptive beam model and dynamic characteristics of magnetorheological materials", *J. Sound Vib.*, **261**(3), 465-481. https://doi.org/10.1016/S0022-460X(02)00985-9.

Wang, Q., Wang, W., Zhuang, X., Zhou, C. and Fan, B. (2021), "Development of an electrostatic comb-driven MEMS scanning mirror for two-dimensional raster scanning", *Micromach.*, **12**(4), 378. https://doi.org/10.3390/mi12040378.

Witvrouw, A. and Mehta, A. (2005), "The use of functionally graded poly-SiGe layers for MEMS aplications", *Mater. Sci. Forum*, **492-493**, 255-260. https://doi.org/10.4028/www.scientific.net/MSF.492-493.255.

Yancheng, L. and Jianchun, L. (2019), "Overview of the development of smart base isolation system featuring magnetorheological elastomer", *Smart Struct. Syst.*, **24**(1), 37-52. https://doi.org/10.12989/sss.2019.24.1.037.

Yang, L., Peng, J., Fang, F. and Yang, J. (2019), "Static pull-in instability and free vibration of functionally graded graphene nanoplatelet reinforced micro-sandwich beams under thermo-electrical actuation", *Microsyst. Technol.*, **25**, 3599-3608. https://doi.org/10.1007/s00542-019-04359-6.

Younis, M.I., Ouakad, H.M., Alsaleem, F.M., Miles, R. and Cui, W. (2010), "Nonlinear dynamics of MEMS arches under harmonic electrostatic actuation", *J. Microelectromech. Syst.*, **19**(3), 647-656. https://doi.org/10.1109/JMEMS.2010.2046624.

Zeerouni, N., Aguib, S., Nour, A., Djedid, T. and Nedjar, A. (2018), "Active control of the nonlinear bending behavior of magnetorheological elastomer sandwich beam with magnetic field", *Vibroeng. Procedia*, **18**, 73-78. https://doi.org/10.21595/vp.2018.19934.

Zhou, G.Y. and Wang, Q. (2006), "Use of magnetorheological elastomer in an adaptive sandwich beam with conductive skins. Part I: Magnetoelastic loads in conductive skins", *Int. J. Solid. Struct.*, **43**(17), 5386-5402. https://doi.org/10.1016/j.ijsolstr.2005.07.042.

CC

Appendix

Due to the conductivity of the skins, by applying the magnetic field, a horizontal force N_j and a distributed moment M_j^m is created in the skins which are expressed as, Zhou and Wang (2006)

$$N_j = \frac{B^2 b h_j}{\mu_{ej}} \frac{\partial^2 u_j}{\partial x^2} \tag{A1}$$

$$M_j^m = \frac{B^2 g h_j}{2\mu_0}\left(\frac{\pi}{\ln\left(\frac{x}{L-x}\right)}\frac{\partial u_j}{\partial x} - \frac{h_j}{\pi}\left(\ln\frac{x}{L-x}\right)\right.$$
$$\left.\frac{\partial^2 w_j}{\partial x^2} + 2\frac{\partial w_j}{\partial x}\right) - \frac{B^2 b h_j^3}{12\mu_{ej}}\frac{\partial^3 w_j}{\partial x^3} \tag{A2}$$

Here, subscripts j=t, b, are for the top and bottom skin layers and B is the magnetic field applied to the sandwich beam and μ_e and μ_0 are the permeability of the skin materials and the free space, respectively. The per unit length electrostatic force f_e is expressed as Huang *et al.* (2001) and here ε_0 is the permittivity of the vacuum that can be written as follow (Farrokhabadi *et al.* 2016)

$$f_e = \frac{\varepsilon_0 v^2}{2}\left(b(g-w)^{-2} + 0.65(g-w)^{-1}\right)$$
$$\varepsilon_0 = 8.854 \times 10^{-12}\ C^2\ N^{-1}\ m^{-2} \tag{A3}$$

v and g are the voltage difference between electrodes and the gap between two electrodes, respectively.

The non-conservative work done due to the applied electrostatic force and the magneto-elastic loads and moments can be given by

$$W_{nc} = \int_0^L (f_e)\delta w\,(x)dx + \int_0^L (N_t\,\delta u_t + N_b\,\delta u_b$$
$$+ M_b^m \delta\frac{\partial w\,(x)}{\partial x} + M_b^m \delta\frac{\partial w\,(x)}{\partial x})dx \tag{A4}$$

Also the variation of the kinetic energy can be written as follows

$$T = \frac{1}{2}\int_0^L m\left(\frac{\partial w\,(x)}{\partial t}\right)^2 dx \tag{A5}$$

Considering the bending and axial load in the skins and the core shearing, the strain energy can be written as follows

$$U = U_{bending} + U_{extension} + U_{shearing}, \tag{A6-a}$$

$$(U_t)_{bending} = \frac{1}{2}\int_0^L E_t I_t \left(\frac{\partial^2 w}{\partial x^2}\right)^2 dx, \tag{A6-b}$$

$$(U_b)_{bending} = \frac{1}{2}\int_0^L E_b I_b \left(\frac{\partial^2 w}{\partial x^2}\right)^2 dx, \tag{A6-c}$$

$$(U_b)_{extension} = \frac{1}{2}\int_0^L E_b A_b \left(\frac{\partial u_b}{\partial x}\right)^2 dx, \tag{A6-d}$$

$$(U_t)_{extension} = \frac{1}{2}\int_0^L E_t A_t \left(\frac{\partial u_t}{\partial x}\right)^2 dx, \tag{A6-e}$$

$$(U_c)_{shearing} = \frac{1}{2}\int_0^L G_c^* A_c \gamma_c^2 dx. \tag{A6-f}$$